INTERFACE SCIENCE 9, 43–53, 2001

Grain Boundary Grooving as an Indicator of Grain Boundary Phase Transformations

JOCHEN SCHÖLHAMMER, BRIGITTE BARETZKY, WOLFGANG GUST AND ERIC MITTEMEIJER
Max-Planck-Institut für Metallforschung, Institut für Metallkunde, Seestr. 92, D-70174 Stuttgart, Germany

BORIS STRAUMAL
Institute of Solid State Physics, Russian Academy of Sciences, Chernogolovka, Moscow District, RU-142432 Russia

Abstract. The atomic force microscopy (AFM) was used to study the grain boundary (GB) groove profiles far away from the melting temperature T_m. It is shown that AFM allows one to measure the temperature dependence of the GB energy in a rather broad temperature interval (from 0.85 T_m to T_m). The GB energy and GB segregation of Bi were measured at 1123 K in the interval of the Bi bulk concentration x^v_{Bi} from 5 to 140 ppm Bi. The transition from monolayer to multilayer adsorption is observed for the Σ19a GB at 1123 K and $x^v_{Bi} = 60$ at. ppm Bi. At the same point (1123 K and $x^v_{Bi} = 60$ at. ppm Bi) a discontinuity of the first derivative of the GB energy is observed. These features were explained using the model of GB prewetting phase transformation developed previously.

Keywords: grain boundaries, thermal groove, segregation, Cu, Bi

1. Introduction

The phase transitions of the first and second order are accompanied, respectively, by discontinuities of the first or second derivative of the free energy. Therefore, the measurement of the energy is the most unambiguous way to find and identify the phase transitions in a system. Encouraged by the success in the investigations of the phase transitions on the free surfaces [1–3], the search on the grain boundary (GB) phase transitions was started in the 80-es. Big efforts in this area resulted in new knowledge in this important branch of physics and materials science. The GB phase transitions can be divided into two main groups.

(1) *Structural GB phase transitions*. These GB phase transitions can proceed in pure one-component materials. They are determined mainly by the energetic and geometric pattern in the GB plane defined by the crystallographic structure and misorientation of both grains. These GB phase transitions are rather insensitive to the kind of material and even to the concentration of the second component [4]. A good example of such phenomena are the "*special GB—general GB*" phase transitions proceeding close to the so-called coincidence misorientations θ_Σ [4–7]. The purely geometrical construction of the coincidence sites lattice (CSL) characterized by the reciprocal density of coincidence sites Σ can be destroyed by the infinitely small deviation $\Delta\theta$ of the misorientation θ from the coincidence misorientation [8, 9]. Nevertheless, physically the GB conserve their special structure due to the appearing of the secondary grain boundary dislocations (SGBDs) compensating the mismatch $\Delta\theta = |\theta_\Sigma - \theta|$. The Burgers vectors of such SGBDs are smaller than the Burgers vectors of the lattice dislocations [8, 9]. They are the unit vectors of the displacement-shift conserving (DSC) lattice which is reciprocal to CSL. The coincidence GBs and GBs containing SGBDs are called "special". They

possess lower energy and extremal properties (mobility, segregation, sliding rate, diffusivity etc.) in comparison with the "general" GBs. By increasing $\Delta\theta = |\theta_\Sigma - \theta|$ the GBs loose their special structure and properties and transform into general ones. If Σ is not too low, the special GBs can loose their special structure and properties not only by increasing $\Delta\theta$ but also by increasing temperature [6, 7]. In other words, the energetic minimum at θ_Σ disappears at increasing temperature. Another example of the structural GB phase transitions is the *GB faceting* [10, 11]. If the mutual misorientation of the grains is fixed, the GB still have two degrees of freedom defining its orientation (inclination). Certain inclinations ϕ correspond to the energetic minima. The GB having an intermediate inclination has a higher energy and tends to "dissolve" into two phases—GB facets of lower energy. Faceting is especially typical for special GBs. In this case the low-energy inclinations often coincide with the close-packed planes in CSL. However, it is not the general rule. For example, the second close-packed 90° plane in $\Sigma 3$ CSL in copper does not correspond to the energetic minimum [12]. Namely, instead of one minimum at 90° two energetic minima appears at 82° and 98° [11]. At this minimum the 9R structure with body-centred cubic (bcc) symmetry exists at GBs in the face-centred cubic (fcc) copper.

(2) "*Chemical*" *GB phase transitions*. For these transitions the presence of the second (or third etc.) component is essential. Such GB phase transitions can be described by additional GB lines in the conventional bulk phase diagrams. The position of these GB lines is rather insensitive to the crystallography of GBs. In case of "chemical" phase transitions the pure GB is replaced by the layer of the second phase. Two main situations are possible. In the first case *at least two bulk phases α and β are in the equilibrium*. If the energy $\gamma_{\alpha\alpha}$ of the GB in the phase α is higher than the energy $2\gamma_{\alpha\beta}$ of two interphase boundaries α/β, a layer of the β-phase has to separate two α-grains one from another replacing the α/α GB. If the β-phase is liquid, such a process is called the GB wetting phase transition. The GB phase transition from the incompletely to completely wetted GB can proceed both by changing temperature T and concentration c. Such transitions are studied experimentally and well documented for many two-and three-component systems like Cu–Bi [13], Al–Sn [14, 15], Zn–Sn [16], Al–Pb–Sn [17], Al–Ga [18], Al–Sn–Ga [18], Fe–Si–Sn [19], Fe–Si–Zn [19–22]. In principle, the β-phase can be solid. Due to the experimental troubles (low rate of the equilibration processes in solids), the reliable experimental data for such "solid phase GB wetting" phase transitions are absent. In the second case *only one phase* (*solid solution*) *can exist in the bulk*. The thermodynamics allows that a stable thin layer of a phase can exist on the GB even if only one phase is stable in the bulk [19, 20, 23, 24]. Such a layer can suddenly appear on the GB as a result of the GB premelting or prewetting phase transition [23, 24]. The model of the GB premelting or prewetting phase transition allowed to explain the extremely high rate of interface and GB diffusion [19–21, 25, 26], the abnormal increase of the GB mobility with increasing impurity content [27], the anomalous GB segregation [28–30], and the presence of a stable thin layer of the second phase in GBs [24]. However, till now the data on the GB prewetting and/or premelting phase transitions were not supported by the results on the derivative discontinuities of the interface or GB energy. The goal of this work is to search for such discontinuities measuring the GB groove profile with the aid of atomic force microscopy (AFM) and simultaneously determining the GB segregation in the Cu–Bi system.

2. Experimental

The bicrystals with a symmetrical $\Sigma 19a$ ⟨011⟩ (133) (26.53°) tilt GB were produced from 99.999 wt.% Cu using the Bridgman technique [31]. Samples of size 3 mm × 3 mm × 15 mm were cut by spark erosion such that the GB was located in the middle of the sample and perpendicular to the surface. The method of vapour transfer was used to obtain Cu samples containing Bi. The samples were etched in an aqueous solution of 50% HNO_3 in order to remove the oxidized film. Each sample was then sealed separately in a silica tube with a Bi vapor source. Differing from the pure Bi source used by Li and Zhang [32], the Cu–Bi alloys were prepared as Bi vapor sources. The compositions of these alloys were Cu–1 wt.% Bi. Alloys of these compositions are in the two-phase region at the annealing temperature. Therefore, the Bi concentration in the Cu bicrystal can increase only up to the concentration of solidus. To the

contrary, a pure liquid Bi source even in a small amount can induce the formation of a liquid phase on a Cu target because in this case the Bi concentration in the Cu bicrystal can increase up to the liquidus concentration [32]. The silica tubes were positioned in the furnace in such a way that the Cu crystals were kept at the desired temperature ($T = 1123$ K) while the temperature of the Cu–Bi alloy was about 5°C higher. Different annealing times for a vapor transfer were chosen in order to produce samples with different Bi content (for example, annealings during 2×10^4, 1.9×10^5 and 6×10^5 s result in $x_{\mathrm{Bi}}^{v} = 38$, 60 and 98 at. ppm Bi, respectively). Subsequently, each sample was water quenched, encapsulated again and homogenized in vacuum for 240 h at 1223 K and water quenched. After this treatment the Bi concentration in the sample was determined by using atomic absorption spectrometry in a Perkin-Elmer spectrometer (model 5000) with the extreme relative accuracy of 10^{-6}.

For the measurements of the GB segregation the specimens were then annealed in vacuum for 110 h at 1123 K. This temperature was chosen using the data of our previous works [28–30] in order to ensure the GB brittle fracture in a broad interval of the bulk Bi concentration. After annealing the specimens were quenched ex situ and then fractured in situ in the ultra high vacuum chamber of a PHI 600 Scanning Auger Multiprobe with a cylindrical mirror analyzer at the temperature of liquid nitrogen. The Bi concentration was measured by means of Auger electron spectroscopy (AES) at 20–30 sites on the fracture surface. The standard methods of the Auger signal processing have been used [33]. In this work we express the Bi concentration at the GBs in monolayers (MLs) of Bi. One ML of pure Bi contains 9.3 atoms/nm^2. The analysis was carried out with the excitation beam normal to the specimens (energy of the primary electron beam was 10 keV). The spectra were taken during argon ion sputtering. The sputtering was accomplished using a 3 keV Ar^+ ion beam. The etching rate was considerably faster than the adsorption rate of the active residual gases. The sputter rates were determined to be 0.52 nm/min relative to Ta_2O_5. The estimated sputter rate for Bi was 1.83 nm/min or 0.178 min/ML. As references were used the pure Cu and Bi. The peak-to-peak intensities were measured for one Bi and two Cu Auger-peaks (Bi: 94–99 eV; Cu: 55–60 eV and 834–921 eV) in dependence on the sputter time.

For the measurements of the GB energy, the surfaces of the pure Cu and Cu–Bi alloys were then prepared by a Reichert-Jung ultramilling machine, in order to produce a microscopically smooth and plane surface. The samples were then encapsulated again and annealed in vacuum for 110 h at 1123 K, to develop the GB grooves, and thereafter water quenched. The topography of the surface in the vicinity of the GB was measured by using a Topometrix 2000 Explorer atomic force microscope. It was operating in the contact mode.

3. Results

A three-dimensional representation of a typical Σ19a GB groove in a Cu bicrystal is shown in Fig. 1. The surface area shown has a size of 50 μm $\times$ 50 μm and a resolution corresponding to 300 $\times$ 300 pixels. A three-dimensional representation of a typical Σ3 GB groove in a Cu polycrystal is shown in Fig. 2. The surface area shown has a size of 20 μm $\times$ 20 μm and a resolution corresponding to 300 $\times$ 300 pixels.

A total of 20 GB groove profiles (height scans over the surface perpendicular to the GB) were evaluated for each sample. Typical profiles for Σ19a and Σ3 are shown in Fig. 3. The profiles of the GB grooves are symmetric. Surface faceting is not present in these grooves. The characteristic shape of the profile provides clear evidence for the surface diffusion mechanism of the groove formation: namely, the symmetric hillocks close to the groove are formed only when the atoms leaving the groove tip move outwards along the surface and not through the bulk or vapor phase [34–36]. The corresponding dihedral angles and the associated standard deviation σ were calculated.

The dihedral angle θ of the GB groove is determined by the condition of mechanical equilibrium at the groove root [37]:

$$\gamma_{\mathrm{gb}} = 2\gamma_{\mathrm{sur}} \cos\frac{\theta}{2} \tag{1}$$

where γ_{sur} and γ_{gb} are the surface energy and the GB energy, both per unit area, respectively. To obtain θ from the measured data, the experimentally determined GB groove profiles were (i) fitted with an analytical expression based on the theory due to Mullins [34] and (ii) differentiated by a direct numerical method described in detail in [38].

The profile of a GB groove formed by surface diffusion was described theoretically by Mullins [34], employing the Gibbs-Thompson equation and assuming a nearly planar groove surface. Then it holds that the groove profile as a function of time obeys the same

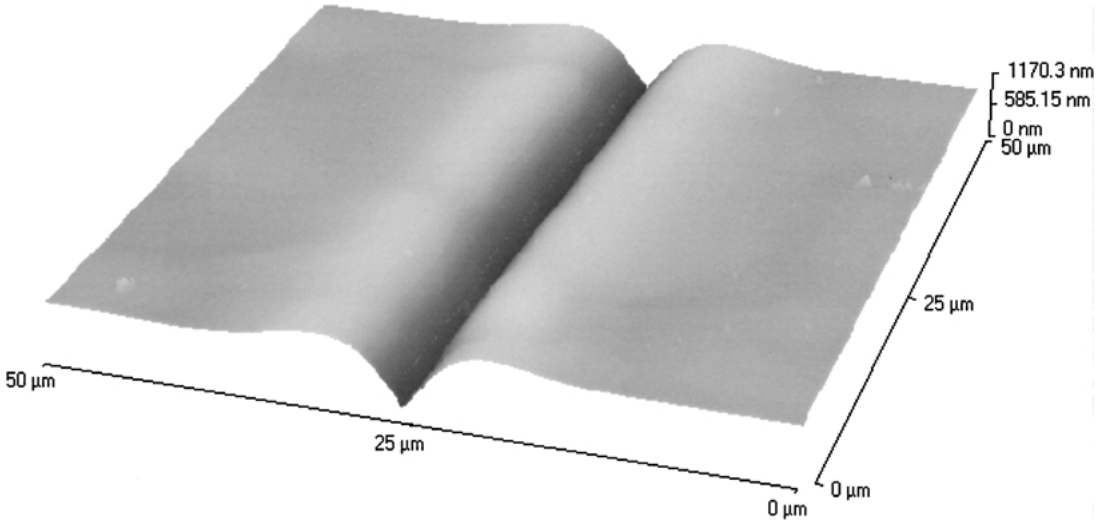

Figure 1. AFM image of a Σ19a GB groove of a Cu bicrystal annealed for 110 h at 1123 K.

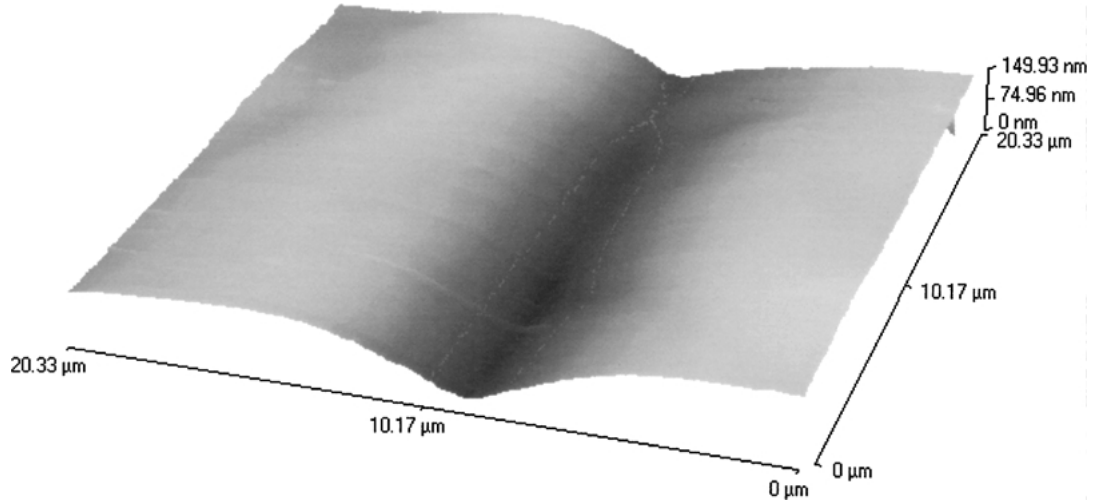

Figure 2. AFM image of a Σ3 GB groove of a Cu polycrystal annealed for 110 h at 1123 K.

shape function as follows. Consider a cross-section of a GB groove and define a two-dimensional Cartesian coordinate system in the cross-sectional plane such that the x-axis coincides with the initially flat surface and the z-axis coincides with the GB. Since the groove is symmetric with respect to the z-axis, it is sufficient to describe $z(x, t)$ for $x \geq 0$ only. According to [34]:

$$z(x, t) = m(At)^n Z\left(\frac{x}{(At)^n}\right) \tag{2}$$

where m is the slope of the GB groove at $x = 0$ (incorporating the effect of γ_{gb} and determined by the dihedral angle θ) and t is the annealing time. For the GB groove formed by surface diffusion it holds that $n = \frac{1}{4}$ and that A is given by

$$A = \frac{D_s \gamma_s \nu \Omega^2}{kT} [\mathrm{m}^4\ \mathrm{s}^{-1}] \tag{3}$$

where D_s is the surface diffusion coefficient, ν is the number of atoms/m^2 of surface, Ω is the atomic volume

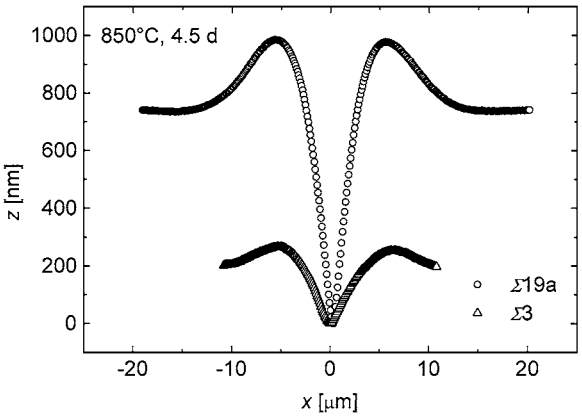

Figure 3. GB groove profiles measured by means of AFM of a Cu bicrystal (Σ19a GB) and a Cu polycrystal (Σ3 GB) annealed for 110 h at 1123 K.

and T is the annealing temperature. $Z(\omega)$ is given by

$$Z(\omega) = \sum_{i-0}^{\infty} a_i \omega^i \quad \text{where } \omega = \frac{x}{(At)^n} \tag{4}$$

with the coefficients

$$\begin{aligned} a_0 &= \frac{-1}{\sqrt{2}\Gamma(5/4)}[a_1 - 6\Gamma(1/2)a_3], \quad a_1 = 1, \\ a_2 &= \frac{-1}{2\sqrt{2}\Gamma(3/4)}[a_1 + 6\Gamma(1/2)a_3], \quad a_3 = 0 \end{aligned} \tag{5}$$

and

$$a_{i+4} = a_i \frac{i-1}{4(i+1)(i+2)(i+3)(i+4)}$$

where $\Gamma(u)$ is the gamma function. Because the specimens were annealed only for a certain time and at a certain temperature the factor $(At)^n$ can be considered as a constant parameter B. If follows from Eq. (2) that the maximal height, denoted by $h_0 + \Delta h$, of the calculated profile is given by

$$h_0 + \Delta h = 0.974 m(At)^n \tag{6}$$

where h_0 is the difference between the measured height maximum and the measured height minimum (see Fig. 3) and Δh is a fitting parameter that can be conceived to incorporate correction for GB groove root blunting effects, discussed in Section 3. Substitution of $m(At)^n$ according to Eq. (6) into Eq. (2) leads to:

$$z(x) = \frac{h_0 + \Delta h}{0.974} Z\left(\frac{x}{B}\right) \tag{7a}$$

Because the height of the initial surface is unknown, the experimentally determined height z' differs from the true height z according to:

$$z'(x) = z(x) + c = \frac{h_0 + \Delta h}{0.974} Z\left(\frac{x}{B}\right) + c \tag{7b}$$

It follows for $x = 0$:

$$-\Delta h = \frac{h_0 + \Delta h}{0.974}(-0.780) + c \tag{8}$$

Finally, substitution of c according to Eq. (8) into Eq. (7b) gives:

$$z'(x) = \frac{h_0 + \Delta h}{0.974} Z\left(\frac{x}{B}\right) + 0.801 h_0 - 0.199 \Delta h \tag{9}$$

The thermal grooving method does not allow to separate γ_{gb} and γ_{sur} and, therefore, permits to measure only the ratio of GB and surface energy γ_{gb}/γ_{sur}. In Fig. 4(a) the dependence of the ratio γ_{gb}/γ_{sur} on the bulk concentration of Bi is shown. The dependence $\gamma_{gb}/\gamma_{sur}(x^v_{Bi})$ can be subdivided into three parts marked by arrows. (1) Quick increase of γ_{gb}/γ_{sur} from 0.45 to 0.65 in the concentration interval from $x^v_{Bi} = 0$ to 10 at. ppm Bi. This unusual behaviour can be explained by the transition from the monolayer to the multilayer adsorption on the free surface (see also the Section 4). (2) Almost constant $\gamma_{gb}/\gamma_{sur} = 0.67$–$0.68$ in the concentration interval from $x^v_{Bi} = 10$ to 60 at. ppm Bi. (3) Slow increase of γ_{gb}/γ_{sur} from 0.68 to 0.8 in the concentration interval from $x^v_{Bi} = 60$ to 140 at. ppm Bi. In this the concentration interval both the scatter of contact angle θ along the GB and the scatter of points for various x^v_{Bi} are rather high in comparison with the interval *1*.

In Fig. 4(b) the data on GB Bi segregation (GB Gibbsian excess Z^Φ of Bi) are shown in dependence on the bulk Bi concentration x^v_{Bi}. The x^v_{Bi} scale is the same in Fig. 4(a) and (b) making easier the comparison of data of GB energy and segregation. The $Z^\Phi(x^v_{Bi})$ plot can be subdivided into two parts. The transition between them is marked by an arrow. (1) In the concentration interval from $x^v_{Bi} = 0$ to 60 at. ppm Bi the GB concentration increases slowly and remains below 1 ML (monolayer adsorption). (2) At $x^v_{Bi} = 60$ at. ppm Bi the GB concentration Z^Φ starts to increase again

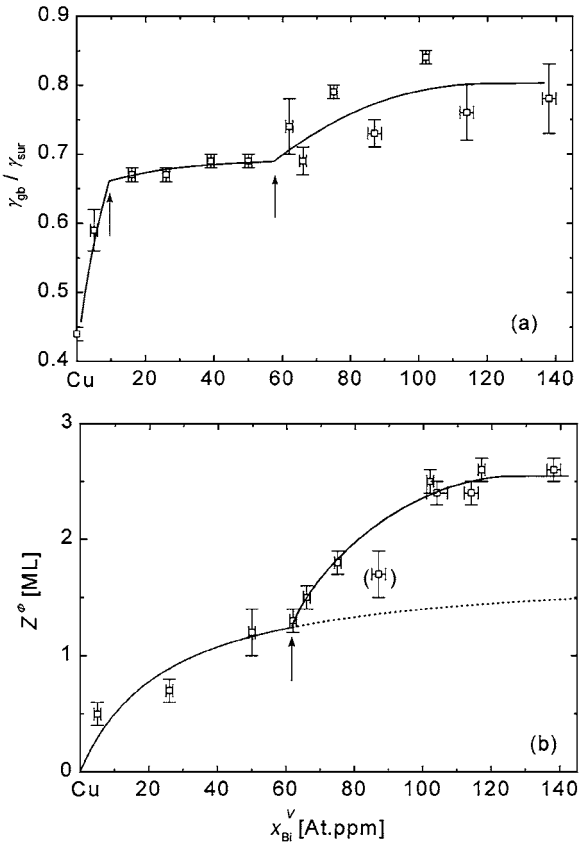

Figure 4. (a) The ratio of the energy γ_{gb} of the Σ19a GB to the energy γ_{sur} of the free surface measured at 1123 K in Cu(Bi) bicrystals with various Bi bulk concentrations. (b) Bi GB segregation as a function of Bi bulk concentration in the Σ19a Cu(Bi) bicrystals.

and reaches the value of $Z^{\Phi} = 2.5$ ML at $x^{v}_{Bi} = 140$ at. ppm Bi (multilayer adsorption).

4. Discussion

A thermal GB groove forms at the intersection of a GB and the surface as a result of the strive for lower energy by reduction of interfacial area. Possible mechanisms leading to GB groove formation are surface diffusion, volume diffusion, and local evaporation and condensation [34–36]. The dihedral angle of GB grooves has often been used to determine interfacial energies, as well as surface and volume diffusion coefficients from the kinetics of the groove deepening [25, 26, 34, 39]. So far, GB groove profiles were measured by using optical interferometric microscopy [12, 40, 41]. The application of interferometric microscopy requires a straight GB groove with a length of several mm. The lateral resolution of this method is of the order of the wavelength of the light applied (i.e. $\approx$500 nm). Therefore, it was possible to measure the GB profile only very close to the melting temperature T_m (about 0.97 T_m [12, 40, 41]) because only at high temperature the diffusion rate is high enough to develop the measurable GB groove after a reasonable annealing time. Contrary to these conventional methods for GB groove profile measurement, atomic force microscopy [42] could enable an easy non-destructive measurement of the GB groove surface topography with a possible atomic height resolution and a lateral resolution as small as several nm. Thereby, the dihedral angle at the root of the GB groove could be measured with a much higher accuracy than it is possible with conventional methods.

The comparison of Figs. 1 to 3 shows that AFM permits to measure the grooves rather far away from T_m (namely, the annealing temperature $T = 1123$ is about 0.85 T_m for Cu). Even at this temperature of 0.85 T_m AFM permits to resolve very well the rather small difference of γ_{gb} for low-energy symmetrical twin Σ3 and coincidence Σ19a GBs. Therefore, the AFM allows to study the temperature dependence of the GB energy in metals in the temperature interval from T_m to at least 0.8–0.85 T_m. According to our knowledge, the successful measurements of the GB thermal grooves far away from T_m were previously performed only in ceramics [43–47].

The comparison of Fig. 4(a) and (b) permits one to suppose that a GB phase transition proceeds in the Σ19a GB at $x^{v}_{Bi} = 60$ at. ppm Bi. At this concentration a discontinuity of the GB energy is present (Fig. 4(a)) and the transition from monolayer to multilayer GB segregation occurs (Fig. 4(b)). The scheme in the bottom part of Fig. 5 illustrates the discontinuity of the GB energy γ_{gb} at $x^{v}_{Bi} = 60$ at. ppm Bi where the energies of two GB phases are equal. The metastable continuations of the $\gamma_{gb}(x^{v}_{Bi})$ plots are shown by the dotted lines. The break at $x^{v}_{Bi} = 10$ at. ppm Bi which can be seen in Fig. 4(a), is not present in Fig. 4(b). It can be explained by the fact that the Z^{Φ} value measured by AES is determined only by the GB properties. However, the ratio γ_{gb}/γ_{sur} depends not only on the GB but also on the surface behaviour. If the transition from the monolayer to the multilayer adsorption proceeds not only on the GB but also on the free surface, it has to occur at lower values of x^{v}_{Bi}. The scheme of the $\gamma_{sur}(x^{v}_{Bi})$ plot for such a situation is also shown in the bottom part of Fig. 5. In

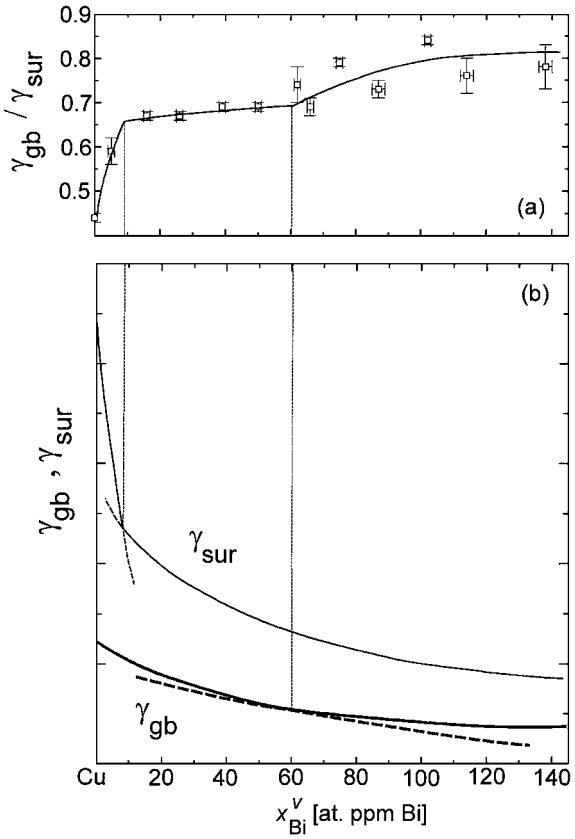

Figure 5. Scheme of the concentration dependence of the GB energy γ_{gb} and surface energy γ_{sur} (a), explaining the quick change of the γ_{gb}/γ_{sur} ratio below 10 at. ppm Bi by the possible prewetting phase transition at the free surface (b).

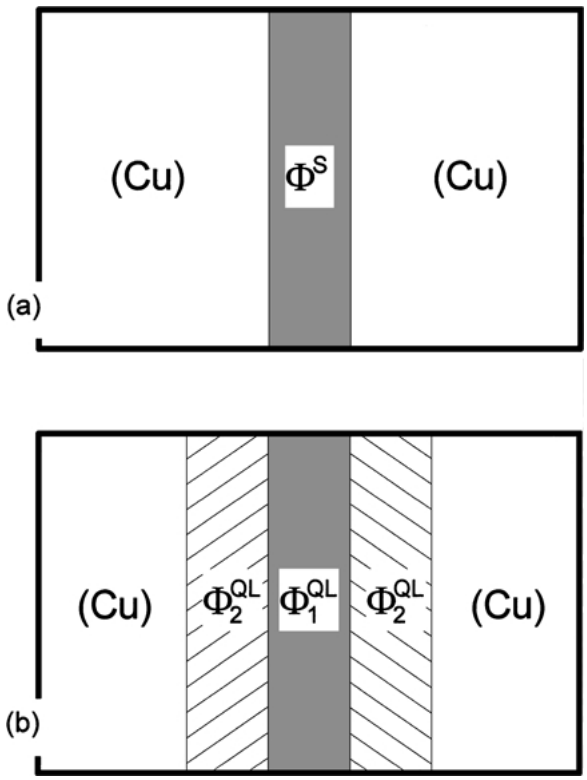

Figure 6. Two possible GB structures: (a) GB with a Bi-enriched solid core and (b) prewetted GB. QL = quasi-liquid.

this case the ratio γ_{gb}/γ_{sur} would contain two breaks, at low and at high x_{Bi}^{v}.

In [28–30] the GB segregation of Bi in Cu polycrystals was measured. Each temperature dependence of Z^{Φ} obtained in [28–30] can also be subdivided into two parts. (1) Low temperature branch with $Z^{\Phi} > 1$ ML. (2) High temperature branch with $Z^{\Phi} < 1$ ML. The Z^{Φ} value at the low temperature branch is almost constant and independent on the temperature, which is not typical for the conventional GB segregation. Above the temperature of the transition from the branch *1* to the branch *2*, the Z^{Φ} value decreased with increasing temperature until the sample did not exhibit any more the brittle GB fracture at about $Z^{\Phi} = 0.3$ ML. It has been shown [30] that the classical Fowler adsorption isotherm fails to describe the GB behavior in the Cu–Bi system. Therefore, the new model of the GB prewetting phase transition was developed in [30].

From the first glance it would be natural to assume that at the GB solidus line the ordered GB core is replaced by a homogeneous layer of the quasi-liquid phase, in the spirit of the Kikuchi-Cahn model [48]. This description meets, however, serious quantitative difficulties. At high temperatures, the concentration of Bi in the Cu–Bi liquid is low (2 to 10 at.% Bi), and one needs to assign a large thickness to the layer of the quasi-liquid phase in order to get the observed value of the GB Gibbsian excess Z^{Φ} of Bi of 1 ML and more (see Fig. 4(b)). Such a thick (about 10 to 100 interatomic distances thick) layer of a quasi-liquid cannot be stabilized by short-range forces from two solid/liquid interfaces and is, therefore, unstable.

In the prewetting model of the GB segregation we assume that the quasi-liquid layer at the GB is thin but inhomogeneous, the Bi-rich core region still having a structure similar to the structure of the untransformed GB core, but being surrounded by two thin layers of a quasi-liquid phase(Fig. 6). Indeed, a thin layer of a quasi-liquid should be strongly modulated by the adjacent crystals [49], and the structure of the GB core

region may be similar to that of the untransformed GB. The driving force for the formation of two quasi-liquid layers surrounding the GB core is the high chemical energy ΔG_{chem} associated with a stepwise change of the Bi concentration at the GB core. According to Lee and Aaronson [50]

$$\begin{aligned}\Delta G_{\text{chem}} &= \left(x_{\text{Bi}}^{\Phi\text{S}} - x_{\text{Bi}}^{(\text{Cu})}\right)^2 n_{\text{s}} Z_{\text{v}} \\ &\quad \times \left(\varepsilon_{\text{Cu-Bi}} - \frac{\varepsilon_{\text{Cu-Cu}} + \varepsilon_{\text{Bi-Bi}}}{2}\right) \\ &= \left(x_{\text{Bi}}^{\Phi\text{S}} - x_{\text{Bi}}^{(\text{Cu})}\right)^2 \Omega^{\text{I}} \qquad (2)\end{aligned}$$

where $x_{\text{Bi}}^{\Phi\text{S}}$, $x_{\text{Bi}}^{(\text{Cu})}$ n_{s} and Z_{v} are the Bi concentration in the GB core and in the bulk, the number of atoms per unit area of the GB core and the coordination number across the GB core, respectively. $\varepsilon_{\text{A-B}}$ is the energy of the atomic A–B bond and Ω^{I} defined by Eq. (2) is the interaction energy across the GB core. The chemical energy is associated with the presence of Cu–Bi bonds across the GB core, which are energetically unfavorable in systems with a high positive enthalpy of mixing. It is this mixing enthalpy which causes the retrograde solubility in the bulk [51, 52].

This approach permitted to describe quantitatively the observed breaks on the $Z^{\Phi}(T)$ dependence and to construct the line of the GB premelting phase transition in the Cu–Bi bulk phase diagram. This phase diagram is shown in the Fig. 7. The bulk solidus (thick line) was experimentally obtained in [51]. The GB solidus (thin line) was calculated basing on the experimental data on Bi segregation in polycrystals [28–30]. The GB solidus represent the GB prewetting phase transition and is completely positioned in the solid solution field of the bulk phase diagram. In Fig. 7 the schemes of the microstructures are also given for three main fields of the phase diagram. At the low concentrations of Bi only the (Cu) phase (Cu-based solid solution) exists in the bulk. The conventional segregation of Bi Φ_{S} is present in the GBs, it means the GBs remain "solid". At the thin retrograde line the GB prewetting phase transition occurs. Between the thin retrograde line (GB solidus) and thick one (bulk solidus) only the solid solution (Cu) is present in the bulk, but GBs contain now the (prewetting) GB phase Φ_{L}. In other words, the bulk remains solid, but the GBs became "liquid". In the two-phase area of the bulk diagram the bulk liquid phase L appears in addition to the (Cu) solid solution. The GBs conserve the same structure Φ_{L}. It is important that the GB liquid-like phase appears at the GB solidus line.

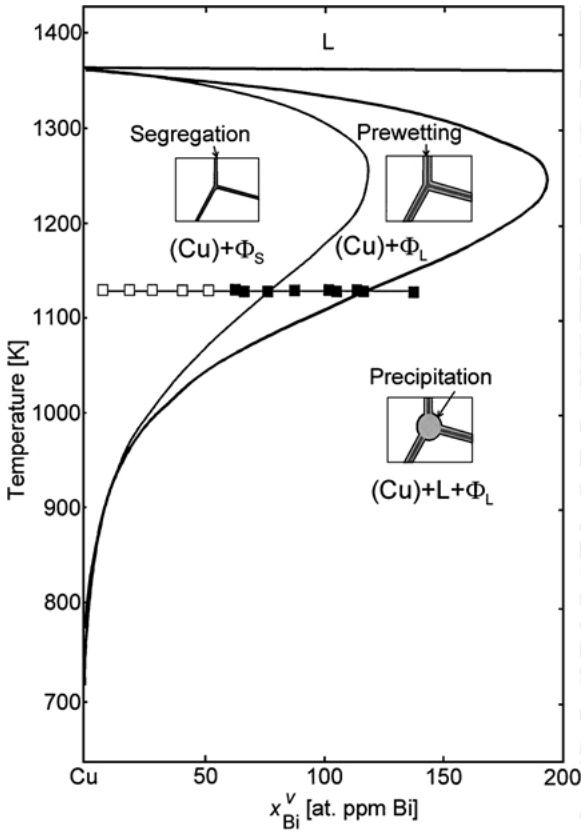

Figure 7. Cu–Bi phase diagram showing the lines of bulk solidus experimentally obtained in [51] and GB solidus for Cu–Bi polycrystals obtained in [29, 30]. The experimental points for the Σ19a GBs studied in this work are also shown. The transition from the open to solid symbols at 60 at. ppm Bi represent the transition from the low-concentration branch to the high-concentration branch on the $\gamma_{\text{gb}}/\gamma_{\text{sur}}(x_{\text{Bi}}^{v})$ and $Z^{\Phi}(x_{\text{Bi}}^{v})$ dependence.

The GB state dose not change principally at the bulk liquidus line when the "true" liquid phase appear in the system. As a result no additional features at $x_{\text{Bi}}^{v} = 120$ at. ppm Bi (concentration of the bulk solidus at 1123 K) can be seen both in the GB energy $\gamma_{\text{gb}}/\gamma_{\text{sur}}(x_{\text{Bi}}^{v})$ and the GB segregation $Z^{\Phi}(x_{\text{Bi}}^{v})$ plots (Fig. 4(a) and (b)). The same behavior was observed in [29, 30], namely the GB segregation of Bi remained unchanged at about $Z^{\Phi} = 2$ ML before and after the intersection with the bulk solidus line.

The GB solidus shown in Fig. 7 was obtained in [29, 30] on polycrystals. By the brittle GB failure of a polycrystal (1) enough brittle GBs have to be present in the polycrystal and (2) the "weakest" GBs are broken. Therefore, the GB solidus obtained with the aid of AES measurements of GB segregation on the failure surface

is resulted from the averaging of GB segregation data on several GBs. For each value of x^v_{Bi} and T the set of GBs is different. In this work the bicrystals were used, and in each experiment the crystallography of the studied GB remains the same. It can be seen in the Fig. 7, that the observed GB transition from Φ_S (open symbols) to Φ_L (solid symbols) at $T = 1123$ K proceeds at lower Bi concentration $x^v_{Bi} = 60$ at. ppm Bi than the same transition observed in the polycrystals ($x^v_{Bi} = 75$ at. ppm Bi). The deviation of the GB solidus from the line obtained in polycrystals was also recently observed for the bicrystals containing the $\Sigma 5$ and near-$\Sigma 5$ GBs [53].

The behaviour of the GB energy is the most reliable thermodynamic criterion for the presence of the GB phase transition. Namely, only in case of the discontinuities of a first or second derivative of the GB energy (in relation to the temperature, pressure, concentration of the second component etc.) on can be convinced that the equlibrium GB phase transition really occurs. Other evidences (like changes in the GB structure, mobility, diffusivity, segregation, strength etc.) are not unambigous and could be driven by metastable processes.

Unfortunately, in the case of GBs, the GB energy cannot be measured directly. In all experimental schemes the ratio of GB energy and the energy of the free surface (vacuum grooving [11, 12, 36, 40, 41]), solid / liquid interface (liquid grooving [13–22, 54]) or other GBs (GB triple junctions [4, 6, 7]) is measured. Therefore, if the discontinuities of the first or second derivative appear in the plots for the ratio of the GB energy and surface or interface energy, the method is needed how to distinguish the GB feature from the artifacts driven by the free surface and/or other interfaces. Fortunately, the GB segregation and kinetic properties of GBs are more sensitive to the GB phase transitions than the GB energy. Therefore, simultaneous measurements of the GB energy ratio and other GB properties allows one to confirm the existence of the GB phase transitions and to exclude possible artifacts driven by the influence of the free surface (vacuum grooving), solid/liquid interface (liquid grooving) or other GBs (GB triple junctions) on the energy ratio. For example, in this work the comparison of γ_{gb}/γ_{sur} (x^v_{Bi}) and $Z^{\Phi}(x^v_{Bi})$ plots permitted to exclude the feature at low x^v_{Bi} driven by the change of the surface energy which is not present in the $Z^{\Phi}(x^v_{Bi})$ plot.

Previously, the GB phase transitions "special GB—general GB" were observed by the comparison, on the one hand, of the measurements of GB energy made with the aid of the vacuum groove [39] and triple junctions [4, 6, 7] and, on the other hand, of GB structure [8, 9] and GB kinetic properties like mobility [6] and GB diffusion [55]. GB faceting phase transitions were observed by the comparison of the GB energy measurements done with the aid of vacuum grooving [11, 12, 40, 41] and studies of GB microstructure [10, 11, 41]. GB wetting phase transitions of the first order were observed using precise measurements of the temperature and pressure dependence of the GB contact angles in the solid/liquid grooves [13–22]. The occurrence of the GB phase wetting transitions was supported by the investigations of the structure and properties of the two-phase polycrystals [49, 56, 57].

The hypothesis on the "chemical" GB phase transitions in the one-phase area of the bulk phase diagrams (premelting and prewetting phase transitions) allowed to explain the extremely high rate of interface and GB diffusion [19–21, 25, 26], the abnormal increase of the GB mobility with increasing impurity content [27], the anomalous GB segregation [28–30] and the presence of stable thin layers of a second phase in GBs [24]. However, till now the data on the GB prewetting and/or premelting phase transitions were not supported by results on the derivative discontinuities of the interface or GB energy. In this work, the hypothesis of the GB prewetting phase transition is for the first time directly supported by the data on discontinuity of the GB energy derivative. Obviously, the further investigations have to be done in the Cu–Bi system. Particularly interesting would be the temperature dependence of the GB energy close to the GB solidus line. Nevertheless, the data presented in the Fig. 4 already evidence rather unambigously the presence of the GB (prewetting) phase transition in the one-phase area of the bulk phase diagram. This transition leads to the formation of the (liquid-like) Bi-rich layer on the GBs in (Cu) solid solution.

5. Conclusions

1. AFM allows to measure the temperature dependence of the GB energy in a rather broad temperature interval (at least from 0.8–0.85 T_m to T_m).
2. It is possible to measure the difference of the GB energy influenced by the change of the Bi concentration in the bulk at 0.85 T_m.
3. The transition from monolayer to multilyaer adsorption is observed for the $\Sigma 19a$ GB at 1123 K and $x^v_{Bi} = 60$ at. ppm Bi. At the same point (1123 K and

$x^v_{\mathrm{Bi}} = 60$ at. ppm Bi) the discontinuity of the first derivative of the GB energy is observed. These facts are explained using the model of GB prewetting phase transformation developed previously [30].

4. The GB (prewetting) phase transition at the Σ19a GB proceeds at lower x^v_{Bi} values in comparison with data obtained previously on polycrystals.

Acknowledgments

Prof. S. Hofmann, Prof. E. Rabkin and Dr. L.-S. Chang are acknowledged for the fruitfull discussions. The financial support of the INTAS Programme (contract 99-1216), Deutsche Forschungsgemeinschaft (contracts Gu 258/12-1, Gu 258/18-1 and Ho 708/15-1), and Copernicus network (contract ERB IC15 CT98 0812) is acknowledged.

References

1. S. Dietrich, in *Phase Transitions and Critical Phenomena*, edited by C. Domb and J.H. Lebowitz (Academic, London, 1988), Vol. 12, p. 2.
2. D. Jasnov, Rep. Prog. Phys. **47**, 1059 (1984).
3. G. de Gennes, Rev. Mod. Phys. **57**, 827 (1985).
4. E.L. Maksimova, E.I. Rabkin, L.S. Shvindlerman, and B.B. Straumal, Acta Metall. **37**, 1995 (1989).
5. B.B. Straumal and L.S. Shvindlerman, Acta Metall. **33**, 1735 (1985).
6. E.L. Maksimova, L.S. Shvindlerman, and B.B. Straumal, Acta Metall. **36**, 1573 (1988).
7. E.L. Maksimova, L.S. Shvindlerman, and B.B. Straumal, Acta Metall. **37**, 2855 (1989).
8. S.E. Babcock and R.W. Balluffi, Phil. Mag. A, **55**, 643 (1987).
9. T.E. Hsieh and R.W. Balluffi, Acta Metall. **37**, 1637 (1989).
10. T.G. Ference and R.W. Balluffi, Script. Metall. **22**, 1929 (1988).
11. F. Ernst, M.W. Finnis, A. Koch, C. Schmidt, B. Straumal, and W. Gust, Z. Metallk. **87**, 911 (1996).
12. T. Muschik, W. Laub, M.W. Finnis, and W. Gust, Z. Metallk. **84**, 596 (1993).
13. B. Straumal, T. Muschik, W. Gust, and B. Predel, Acta Metall. Mater. **40**, 939 (1992).
14. B. Straumal, D. Molodov, and W. Gust, J. Phase Equilibria **15**, 386 (1994).
15. B. Straumal, W. Gust, and D. Molodov, Interface Sci. **3**, 127 (1995).
16. B.B. Straumal, W. Gust, and T. Watanabe, Mater. Sci. Forum **294–296**, 411 (1999).
17. B. Straumal, D. Molodov, and W. Gust, Mater. Sci. Forum **207–209**, 437 (1996).
18. B. Straumal, S. Risser, V. Sursaeva, B. Chenal, and W. Gust, J. Physique **IV 5-C7**, 233 (1995).
19. E.I. Rabkin, V.N. Semenov, L.S. Shvindlerman, and B.B. Straumal, Acta Metall. Mater. **39**, 627 (1991).
20. O.I. Noskovich, E.I. Rabkin, V.N. Semenov, L.S. Shvindlerman, and B.B. Straumal, Acta Metall. Mater. **39**, 3091 (1991).
21. B.B. Straumal, O.I. Noskovich, V.N. Semenov, L.S. Shvindlerman, W. Gust, and B. Predel, Acta Metall. Mater. **40**, 795 (1992).
22. B. Straumal, E. Rabkin, W. Lojkowski, W. Gust, and L.S. Shvindlerman, Acta Mater. **45**, 1931 (1997).
23. E.I. Rabkin, L.S. Shvindlerman, and B.B. Straumal, Int. J. Mod. Phys. B **5**, 2989 (1991).
24. R.H. French, H. Müllejans, D.J. Jones, G. Duscher, R.M. Cannon, and M. Rühle, Acta Mater. **46**, 2271 (1998) and references therein.
25. E.I. Rabkin, L.S. Shvindlerman, and B.B. Straumal, J. Less-Common Met. **158**, 23 (1990).
26. E.I. Rabkin, L.S. Shvindlerman, and B.B. Straumal, J. Less-Common Met. **159**, 43 (1990).
27. D.A. Molodov, U. Czubayko, G. Gottstein, L.S. Shvindlerman, B.B. Straumal, and W. Gust, Phil. Mag. Lett. **72**, 361 (1995).
28. L.-S. Chang, E. Rabkin, B. Straumal, P. Lejcek, S. Hofmann, and W. Gust, Scripta Mater. **37**, 729 (1997).
29. L.-S. Chang, E. Rabkin, B.B. Straumal, S. Hofmann, B. Baretzky, and W. Gust, Defect Diff. Forum **156**, 135 (1998).
30. L.-S. Chang, E. Rabkin, B.B. Straumal, B. Baretzky, and W. Gust, Acta Mater. **47**, 4041 (1999).
31. P.W. Bridgman, Proc. Am. Ac. Arts Sci. **58**, 163 (1923).
32. Q.-H. Li and L.-D. Zhang, Acta Met. Sinica, **31**(3), 130 (1995) (in Chinese).
33. L.-S. Chang, Ph.D. thesis, University of Stuttgart, 1998.
34. W.W. Mullins, J. Appl. Phys. **28**, 333 (1957).
35. W.W. Mullins, Trans. AIME **218**, 354 (1960).
36. W.W. Mullins and P.G. Shewmon, Acta Metall. **7**, 163 (1959).
37. C. Herring, *The Physics of Powder Metallurgy* (McGraw-Hill, New York, 1951), p. 143.
38. J. Schoellhammer, L.-S. Chang, E. Rabkin, B. Baretzky, W. Gust, and E.J. Mittemeijer, Z. Metallkd. **90**, 687 (1999).
39. A.N. Aleshin, S.I. Prokofjev, and L.S. Shvindlerman, Scripta Metall. **19**, 1135 (1985).
40. R. Schmelzle, T. Muschik, W. Gust, and B. Predel, Scripta Metall. **25**, 1981 (1991).
41. U. Wolf, F. Ernst, T. Muschik, and M.W. Finnis, Phil. Mag. A **66**, 991 (1992).
42. B. Baretzky, B. Reinsch, U. Täffner, G. Schneider, and M. Rühle, Z. Metallk. **87**, 332 (1996).
43. C.A. Handwerker, J.M. Dynys, R.M. Cannon, and R.L. Coble, J. Amer. Ceram. Soc. **73**, 1365 and 1371 (1990).
44. A. Tsoga and P. Nikolopoulos, J. Amer. Ceram. Soc. **77**, 954 (1994).
45. E. Saiz, R.M. Cannon, and A.P. Tomsia, Acta Mater. **47**, 4209 (1999).
46. D.M. Saylor and G.S. Rohrer, J. Amer. Ceram. Soc. **82**, 1529 (1999).
47. D.M. Saylor, D.E. Mason, and G.S. Rohrer, J. Amer. Ceram. Soc. **83**, 1226 (2000).
48. R. Kikuchi and J.W. Cahn, Phys. Rev. B **36**, 418 (1987).
49. J. Howe, Phil. Mag. A **74**, 761 (1996).
50. Y.W. Lee and H.I. Aaronson, Acta Metall. **28**, 539 (1980).
51. L.-S. Chang, B.B. Straumal, E. Rabkin, W. Gust, and F. Sommer, J. Phase Equilibria **18**, 128 (1997).

52. R.A. Swalin, *Thermodynamics of Solids* (John Wiley & Sons, New York, 1972), p. 184.
53. B. Straumal, S.I. Prokofjev, L.-S. Chang, N.E. Sluchanko, B. Baretzky, and W. Gust, Defect Diff. Forum 194–199 (2001).
54. N. Eustatopoulos, L. Coudurier, J.C. Joud, and P. Desre, J. Cryst. Growth **33**, 105 (1976).
55. E. Budke, T. Surholt, S.I. Prokofjev, L.S. Shvindlerman, and Chr. Herzig, Acta Mater. **47**, 385 (1999).
56. B. Joseph, F. Barbier, G. Dagoury, and M. Aucouturier, Scripta Mater. **39**, 775 (1998).
57. B. Joseph, F. Barbier, and M. Aucouturier, Scripta Mater. **40**, 893 (1999).